Physica B 660 (2023) 414901

Contents lists available at ScienceDirect

Physica B: Condensed Matter

journal homepage: www.elsevier.com/locate/physb

Interparticle magnetic interactions and magnetic field dependence of superparamagnetic blocking temperature in ferrihydrite nanoparticle powder systems

A.A. Krasikov [a,*], Yu. V. Knyazev [a,**], D.A. Balaev [a,b], D.A. Velikanov [a], S.V. Stolyar [a,b,c], Yu. L. Mikhlin [d], R.N. Yaroslavtsev [a,c], R.S. Iskhakov [a]

[a] Kirensky Institute of Physics, Federal Research Center KSC SB RAS, Krasnoyarsk, 660036 Russia
[b] Siberian Federal University, Krasnoyarsk, 660041, Russia
[c] Krasnoyarsk Scientific Center, Federal Research Center KSC SB RAS, Krasnoyarsk, 660036, Russia
[d] Institute of Chemistry and Chemical Technology, Federal Research Center KSC SB RAS, Krasnoyarsk, 660036 Russia

ARTICLE INFO

Keywords:
Ferrihydrite nanoparticles
Interparticle magnetic interactions
Superparamagnetic blocking temperature
Coating
Arabinogalactan

ABSTRACT

In this study, nanoparticles of initial synthetic ferrihydrite have been coated with arabinogalactan. The synthesized series of samples with different degrees of coverage of particles has been characterized by X-ray photoelectron spectroscopy, Mössbauer spectroscopy, transmission electron microscopy and magnetometry. The superparamagnetic blocking temperature decreases monotonically with an increase in the degree of coverage of ferrihydrite particles, which is unambiguously related to the different role of the interparticle magnetic interactions in the investigated powder systems. Analysis of the field dependence of the blocking temperature within the random anisotropy model has shown that an increase in the degree of coverage of ferrihydrite particles leads to a decrease in the size of a cluster in which the behaviors of the nanoparticle magnetic moments are correlated. The results obtained have shown the possibility of effective control of the strength of magnetic interparticle interactions in powder ferrihydrite systems by coating nanoparticles with arabinogalactan.

1. Introduction

The wide use of magnetic nanomaterials in various fields is due to the fundamentally new properties inherent to nanosized particles [1–3]. Therefore, the search for new methods for synthesis of materials consisting of magnetic nanoparticles and the establishment of physical mechanisms responsible for the observed properties of the synthesized materials are urgent tasks. The new properties of magnetic nanoparticles include, first of all, the effects related to their developed surface and a large fraction of surface atoms, as well as the effects caused by the "finite" particle size. Studies of such effects in powder systems face another important problem to be solved: how do the interparticle magnetic interactions affect the integral magnetic characteristics of nanoparticle systems? In a nanoparticle ensemble, both the surface and finite-size effects and the interparticle interactions can manifest themselves. In some applications of particle ensembles dispersed in a liquid, the applied magnetic field leads inevitably to aggregation of particles. In systems of interacting and noninteracting particles, the responses to an ac magnetic field or an external field varying with a large gradient will be different. Therefore, the problem of the interparticle magnetic interactions (hereinafter referred to as the interparticle interactions (IPIs)), which was stated long ago, is still being resolved (see, for example [4–10]) and remains a challenge [11–26].

There exist various approaches to establishing the effect of the IPIs and describing the contribution of the IPIs in systems of magnetic nanoparticles. The most of them accounting for processes of transition from superparamagnetic state to so called blocked state of particle magnetic moments. An individual particle, besides its size, characterizes a constant of magnetic anisotropy K. If magnetic anisotropy energy K·V (V – is the particle volume) prevails over thermal energy k·T (k – is the Boltzmann constant) the particle magnetic moment is in the blocked state, in the contrary case term superparamagnetic (hereinafter – SPM) state is used. With varying of temperature, at some characteristic temperature T_B, which is called the blocking temperature, transition from

* Corresponding author.
** Corresponding author.
E-mail addresses: KAA3000@yandex.ru (A.A. Krasikov), yuk@iph.krasn.ru (Yu.V. Knyazev).

https://doi.org/10.1016/j.physb.2023.414901
Received 16 January 2023; Received in revised form 31 March 2023; Accepted 14 April 2023
Available online 14 April 2023

one state to another state occurs.

The IPIs manifest themselves experimentally in magnetic nanoparticle systems as a significant increase in the SPM blocking temperature observed in a fairly weak external field. This can be roughly explained by an additional contribution of energy of the IPIs to the magnetic anisotropy energy K·V. This approach suggests that the interaction of the magnetic moments of particles forms their mutual arrangement that prevents the reversal of their magnetic moments under the action of thermal fluctuations [14]. As a result, the transition from blocked to the SPM state occurs at more temperature than for the case of non-interacting particles, i. e, T_B value growths in the presence of IPIs.

There exists another approach to the analysis of systems of interacting magnetic particles, which is based on the fact that the behaviors of the magnetic moments of particles, due to the presence of the IPIs, are correlated in a certain volume. In this case, the magnetic anisotropy energy K·V will include, instead of the volume of an individual particle, a certain "effective" volume of a cluster consisting of a certain number of particles. It is clear that, in this case, the SPM blocking temperature of a system of particles will increase over the value for noninteracting particles, which is observed in the experiment. If the SPM blocking processes are investigated in different external fields, then the SPM blocking temperature decreases with an increase in the field. For systems of interacting particles, this decrease should be accompanied by a decrease in the size of a cluster in which the magnetic moments of particles behave in a correlated manner. The latter is due to the fact that the Zeeman energy $\mu_P \cdot H$ (μ_P is the particle magnetic moment) not only prevails over thermal fluctuations, but also exceeds the IPI energy. Therefore, in a sufficiently strong external field, the cluster "effective" size should approach the particle size and the SPM blocking temperature should approach the value for the corresponding system of noninteracting particles. This idea was developed in Ref. [27] and called the random anisotropy model (RAM) by its authors, who derived the equation for the field dependence of the size of a cluster with the correlated particle magnetic moments and obtained the field dependence of the SPM blocking temperature ($T_B(H)$) for systems of interacting particles. The RAM was used to analyze the experimental $T_B(H)$ dependences for thin film systems of cobalt [27] and magnetite [28] nanoparticles, as well as for a bulk system of magnetite nanoparticles dispersed in paraffin [21]. In recent study [29], this model was extended to the description of the experimental temperature dependences of the magnetization and coercivity.

Obviously, the IPI effect should be the brightest in systems of ferro- and ferrimagnetic nanoparticles with a typical particle of magnetic moment μ_P of $(10^3–10^4)\mu_B$, where μ_B is the Bohr magneton. Nanoparticles of antiferromagnetic (AFM) materials also have a magnetic moment, although smaller: $\mu_P \sim 10^2\mu_B$. The magnetic moments of AFM nanoparticles are induced by structural defects, which cause an imbalance of ferromagnetically ordered sublattices [13,30–46]. Despite the smaller μ_P value, the effect of the IPIs on the magnetic properties of AFM nanoparticle systems was noted in many works [7,11–13,17,44–46]; as a rule, these were powder systems of AFM nanoparticles contacting fairly close. The IPI value can be tuned (downwards) by the dispersion of magnetic nanoparticles in a nonmagnetic medium [21] or by coating nanoparticles with a nonmagnetic shell [12,14,16,17,23,47,48].

Ferrihydrite (nominal chemical formula $5Fe_2O_3{\cdot}9H_2O$) is a hydroxide which exists only on the nanoscale with typical mean sizes of nanoparticles about 2–5 nm [31–34,36,39,43–47]. Magnetic moments of iron in ferrihydrite are ordered antiferromagnetically and the net magnetic moment of a nanoparticle arises from uncompensated moments of sublattices. There are several methods of preparation of ferrihydrite [31, 33,36,43–46]; also, low-temperature annealing of ferrihydrite results in slight growth of the size of nanoparticles [43]. The purpose of this study is to find a simple way to modify the strength of IPIs in powder systems of ferrihydrite nanoparticles. In this study we suggest to use polysaccharide arabinogalactan as a coating agent. The aim was to detect changes in the experimental $T_B(H)$ dependence upon variation in the degree of coverage of a particle and to establish the contribution of the IPIs to the SPM blocking processes. The obtained $T_B(H)$ dependences were interpreted within the RAM [27,28].

2. Experimental

An initial synthetic ferrihydrite sample was obtained by hydrolysis of iron (III) nitrate. The $Fe(NO_3)_3{\cdot}9H_2O$ solution (0.2 M) with a volume of 100 ml was added with the NaOH solution (1 M) dropwise at a rate of 20 ml/min at room temperature under continuous stirring until neutral pH. The process resulted in the formation of a dark-brown suspension. The precipitate was washed with deionized water to remove remaining ions and dried at room temperature. This sample hereinafter referred to as FH-0 was a powder of agglomerated ferrihydrite nanoparticles.

To obtain nanoparticles coated with arabinogalactan (AG), the as-prepared suspension of ferrihydrite nanoparticles with a volume of 100 ml was added with 0.5–1.5 g of AG (15 mg/ml), which was followed by sonication for 10 min (22 kHz, 50 W/cm^2). Three samples with different AG concentrations and, consequently, different degrees of coverage were obtained, which are hereinafter referred to as FH-1, FH-2, and FH-3, where the numbers correspond to the relative degree of AG coverage. The above-described process regulation ensures the identical sizes of individual ferrihydrite nanoparticles in the initial (FH-0) and coated (FH-1, FH-2, and FH-3) samples.

The transmission electron microscopy (TEM) study was carried out on a Hitachi HT7700 transmission electron microscope at an accelerating voltage of 100 kV. Specimens were prepared by shaking the nanoparticle powder in alcohol in an ultrasonic bath and depositing the obtained suspension onto support meshes with a perforated carbon coating.

X-ray photoelectron spectra (XPS) were recorded with a SPECS instrument (SPECS GmbH, Germany) equipped with a PHOIBOS 150 MCD-9 analyzer operating at a pass energy of 20 eV for survey spectra and 10 eV for high-resolution spectra; the excitation was made using monochromatic Al Kα radiation (1486.7 eV) of an X-ray tube. The pressure in an analytical chamber was around 10^{-9} mbar. The atomic concentrations were determined from the survey spectra. The high-resolution spectra were fitted with the Gaussian–Lorentzian peak profiles after subtracting the Shirley-type background. The Fe 2p spectra were fitted using sets of multiplet lines (four narrow peaks and a wider satellite for Fe^{3+} cations), keeping their relative positions and intensities and varying their widths and binding energy (BE) of the set as a whole [49] in the CasaXPS software.

Mössbauer spectra were obtained on an MS-1104Em spectrometer (manufactured at the Research Institute of Physics, Southern Federal University, Russia) in the transmission geometry with a Co^{57}(Rh) radioactive source in the temperature range of 4–300 K using a CFSG-311-MESS cryostat with a sample in the exchange gas based on a closed-cycle Gifford–McMahon cryocooler (Cryotrade Engineering).

The temperature dependences of the magnetization M(T) were measured with homemade facilities working at Kirensky Institute of Physics, Krasnoyarsk, Russia: a SQUID magnetometer (in external fields of 1–1000 Oe) and a vibrating sample magnetometer (in fields of 10–30 kOe). The zero field cooling (ZFC) and field cooling (FC) modes were used. In the magnetic measurements, the investigated powder was fixed in paraffin in a measuring capsule. Data on the magnetic moment are given in emu units reduced to the mass of the sample.

3. Methodological background

3.1. Standard expressions for SPM blocking

The expression linking magnetic anisotropy constant and SPM blocking temperature T_B is based on the Néel–Brown equation for characteristic time τ of the reversal of the particle's magnetic moment:

$$\tau = \tau_0 \cdot \exp(KV / kT). \quad (1)$$

In Eq. (1), τ_0 is the particle relaxation time (10^{-9}–10^{-13} s). To analyze the experimental data, it is convenient to rewrite Eq. (1) in the form

$$T_B = K \cdot V / \ln(\tau_m / \tau_0) \cdot k. \quad (2)$$

Here, τ_m is the characteristic time of the experimental technique (i.e., T_B value depends on τ_m): τ_m ~10–100 s for static magnetic measurements and $\tau_m \sim 1/\nu$ for the ac magnetic susceptibility. Equation (2) is valid only for noninteracting particles. If dependence (2) obtained from experiment is valid at reasonable τ_0 values (10^{-9}–10^{-13} s), then the IPIs in a system of magnetic nanoparticles are absent and, conversely, the more the τ_0 value extends beyond the specified range (as a rule, becomes unphysically small), the stronger the IPI effect.

For systems of interacting particles, instead of Eq. (2), experimental data are often treated by the following expression

$$T_B - T_0 = K \cdot V / \ln(\tau_m / \tau_0) \cdot k, \quad (3)$$

which is known as so called Wogel-Fulcher law. In expression (3) the larger T_0 values at the τ_0 value lying within the reasonable range (10^{-9}–10^{-13} s) correspond to the stronger IPI contribution. This approach makes it possible to qualitatively describe the experimental data, although the quantitative interpretation of the obtained T_0 values can be complicated. Moreover, the energy $k \cdot T_0$ can both characterize the value of dipole–dipole magnetic interactions and be the energy characteristic in the case of superexchange, when the wave functions of magnetically active atoms of neighboring particles overlap.

3.2. Expressions for analysis within RAM

The field dependence of the blocking temperature for noninteracting particles is described by the following classical relation [27]:

$$T_B(H) = \frac{KV}{k_B \ln(\tau/\tau_0)} \left[1 - \frac{M_S H}{2K}\right]^{3/2}. \quad (4)$$

To analyze the obtained $T_B(H)$ dependences for systems of interacting particles, it would be reasonable to use the RAM approach (see Introduction) suggested in Refs. [27,28]. Within this model [27,28], the size L_H of the cluster in which the magnetic moments of particles behave in a correlated manner depends on the external field, saturation magnetization M_S of a particle, its size D, and parameters A_{eff} and C of the IPI intensity as

$$L_H(H) = D + \sqrt{\frac{2A_{eff}}{M_S H + C}}. \quad (5)$$

It is worth noting that this equation contains the root dependence of the correlation size ~ $H^{-1/2}$ following from the micromagnetic theory [50] and A_{eff} has the same meaning as the exchange constant for nanocrystalline alloys [27,28]. The parameter C is responsible for the intensity of magnetic interactions, inversely proportional to the IPI strength, and plays an important role in weak external fields [28]. With increase of the field H the second term of eq. (5) decreases leading to decrease of L_H and its tending to D value at high fields. The effective volume of particles in the cluster is determined by the volume content of magnetic particles x as $[D^3 + x(L_H - D^3)]$. Instead of anisotropy constant K of an individual particle the RAM deals with the effective anisotropy K_{eff} of the cluster with N particles: $K_{eff} = K/N^{1/2}$. Then, substituting L_H and K_{eff} into (4) one obtains the final equation for the SPM blocking temperature in the RAM:

$$T_B(H) = \frac{\pi K\left[D^3 + x\left(L_H^3 - D^3\right)\right]}{6k_B \ln\left(\frac{\tau_m}{\tau_0}\right)\sqrt{1 + \frac{x\left(L_H^3 - D^3\right)}{D^3}}} \times \left[1 - \frac{M_S H\sqrt{1 + \frac{x\left(L_H^3 - D^3\right)}{D^3}}}{2K}\right]^{\frac{3}{2}}. \quad (6)$$

Note that in this equation K is the magnetic anisotropy constant of an individual particle (disregarding of the IPIs). Equation (6) is written for spherical particles ($V = \pi D^3/6$). The value of the exponent (3/2) in Eq. (5) was argued in Ref. [51]. At $x = 0$ or $A_{eff} = 0$, Eq. (6) transforms to the classical $T_B(H)$ dependence (4) for noninteracting particles.

4. Characterization

4.1. Microstructure characterization

Fig. 1 presents typical microphotographs and microdiffraction patterns obtained by the microstructure study of two samples: initial sample FH-0 and sample FH-3 with the highest degree of coverage of particles. The microdiffraction patterns contain two diffuse reflections corresponding to interplanar spacings of 1.5 and 2.6 Å. Particles in the samples seem visually to have similar sizes and shapes, which is ensured by the sample preparation technique. Average particle sizes <D> obtained from several microphotographs were 2.7 nm and 3.1 nm for samples FH-0 and FH-3, respectively. The somewhat larger <D> value determined for sample FH-3 may be caused by the organic coating of particles, which is hard to distinguish in the micrographs. In addition, the average particle size was estimated using the Scherrer formula. In the calculation, the half-width of the first (brightest) diffraction ring was used (Fig. 1). According to the estimation, the <D> values were found to be identical for both samples: 2.6 nm. Thus, the results obtained confirm the identity of sizes of individual ferrihydrite particles in the initial and AG-coated samples. This, together with the XPS data (Sec. 4.2) and Mössbauer spectroscopy data (Sec.4.3), allows us to consider the particle size distribution to be unchanged for the entire series of the samples. The particle size distribution histogram for initial sample FH-0 is shown in Fig. 1. It can be seen that no particles larger than 3.3 nm were detected. A value of $D_{max} \approx 3.3$ nm will be used to analyze the $T_B(H)$ dependences (Sec. 5.2).

4.2. XPS

The panoramic X-ray photoelectron spectra of the samples obtained at 300 K show the intensities of the iron lines, which decrease in the series FH-0, FH-1, FH-2, FH-3, while the intensities of the carbon lines increase in this series, which is consistent with the expected AG coating thickness. In addition, one can see low-intensity peaks of sodium and calcium impurities, which are indicative of the presence of organic substances. The high resolution spectra of Fe 2p and O 1s are in good agreement with the results obtained for ferrihydrite in Ref. [52]. Let us focus on the high-resolution spectra for the energy ranges corresponding to iron and carbon (Fig. 2).

The Fe $2p_{3/2}$ bands (Fig. 2) can be decomposed quite satisfactorily using a set of multiplet lines (four maxima and a wider satellite) for Fe^{3+} associated with oxygen. Another broad and less intense maximum in the region of 718–720 eV is characteristic of iron oxyhydroxides [49,53]. The relative intensities and energies of the lines coincide with the literature data [49,53], but the linewidth is much larger, which suggests the presence of not one, but several fairly close states of ferri-ions. The total intensity of the maxima changes (it is maximum for sample FH-0 and decreases monotonically in the series FH-1, FH-2, FH-3), according to the series obtained from the survey spectra.

The aforesaid is confirmed by the oxygen and carbon spectra, which are also shown in Fig. 2. The C 1s spectra can be decomposed into three maxima corresponding to carbon sp^3-hybridization (a binding energy of

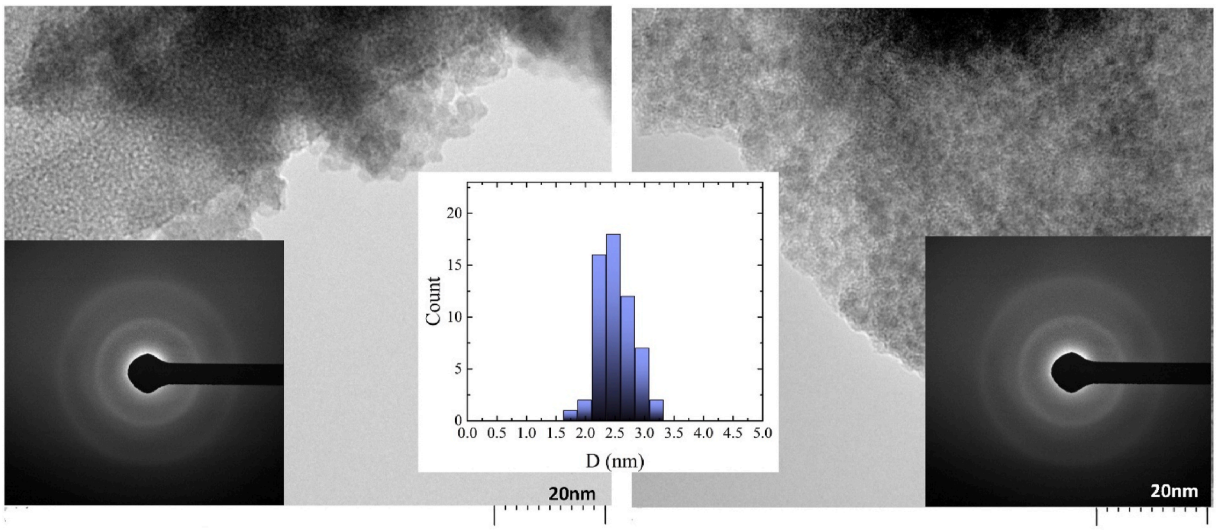

Fig. 1. Typical TEM images and microdiffraction patterns for samples FH-0 (on the left) and FH-3 (on the right) and particle size distributions for sample FH-0 (at the center).

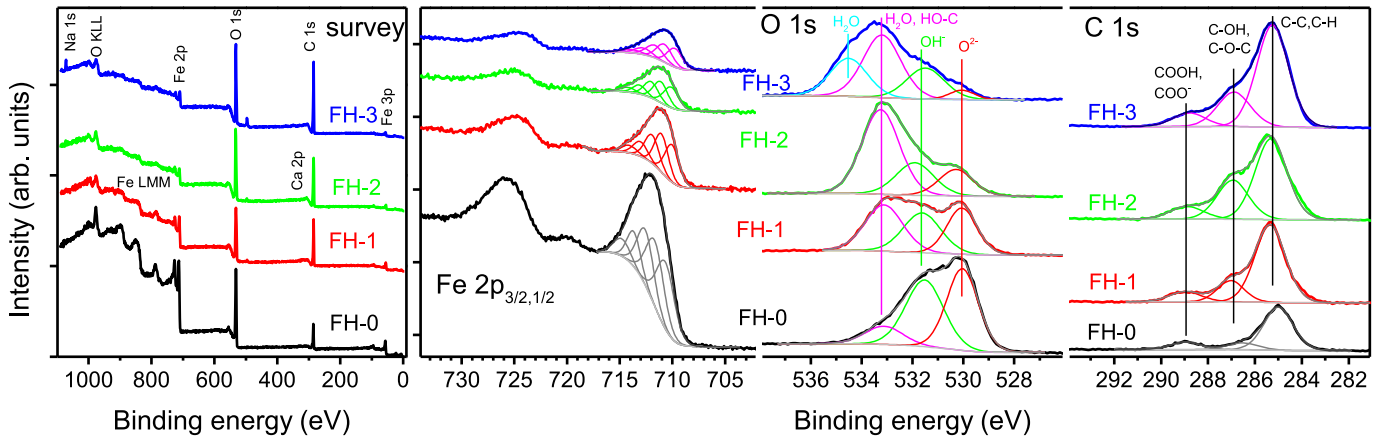

Fig. 2. X-ray photoelectron spectra (survey and narrow scans) of the samples of ferrihydrite nanoparticles synthesized with different amounts of AG.

~285 eV), C–OH groups, possibly C–O–C groups typical of carbohydrates (a binding energy of ~286.5 eV), and weaker components with an energy of ~288.8 eV typical of carboxyl groups. There is carbon, in addition, on the surface of chemically synthesized ferrihydrite as an unavoidable contamination, but the total intensity and the contribution of COH lines increase noticeably with the amount of added AG. The ferrihydrite oxygen spectra contain lines comparable in intensity with the line O^{2-} (~530 eV) and OH^{-} (~531.5 eV), as well as the contributions of oxygen in organic matter and adsorbed water at high binding energies. With an increase in the AG additives, the intensity of the line O^{2-} decreases, while the intensity of COH groups (533.2 eV) grows rapidly. Thus, the changes observed in the Fe 2p, O 1s, and C 1s spectra are indicative of the formation of an organic coating of ferrihydrite nanoparticles, the thickness of which increases partially with the amount of added AG, while the state of particles themselves does not significantly change.

4.3. Mössbauer spectroscopy

Mössbauer spectra of ferrihydrite samples FH-0, FH-1, FH-2, and FH-3 are presented in Fig. 3. At room temperature, each spectrum represents a doublet described by the superposition of three components corresponding to the three nonequivalent iron positions Fe1, Fe2, and Fe3 in ferrihydrite [54–56]. In all the positions, iron cations are in the high-spin trivalent state. The ratio between the relative populations of these doublets in the spectra of all the samples is almost identical and close to 3:2:1. In the case of magnetic nanoparticles, the doublet is a manifestation of the SPM state of the particle magnetic moments [45,47,57–59]. A decrease in temperature leads to the occurrence of a hyperfine structure of the spectrum (Fig. 3), which is a sign of the blocked state of the particle magnetic moments in the Mössbauer technique [13,57–59]. For the spectra at $T = 4.2$ K, the mathematical processing also showed the three characteristic iron positions (Fe1, Fe2, and Fe3) in the octahedral environment with different quadrupole splittings (QS). The relative occupancy of positions Fe1, Fe2, and Fe3 is similar to the data obtained at T = 300 K and independent of the degree of coverage of nanoparticles (Table 1).

Thus, according to the Mössbauer spectroscopy data, the samples are powder systems of ferrihydrite nanoparticles and the similarity of the Mössbauer parameters for them (Table 1) suggests the identity of the properties of individual ferrihydrite particles in the samples. This, together with the TEM and XPS data, allows us to consider the magnetic properties of individual particles to be the same for all the samples in the subsequent static magnetometry analysis of the SPM blocking temperatures.

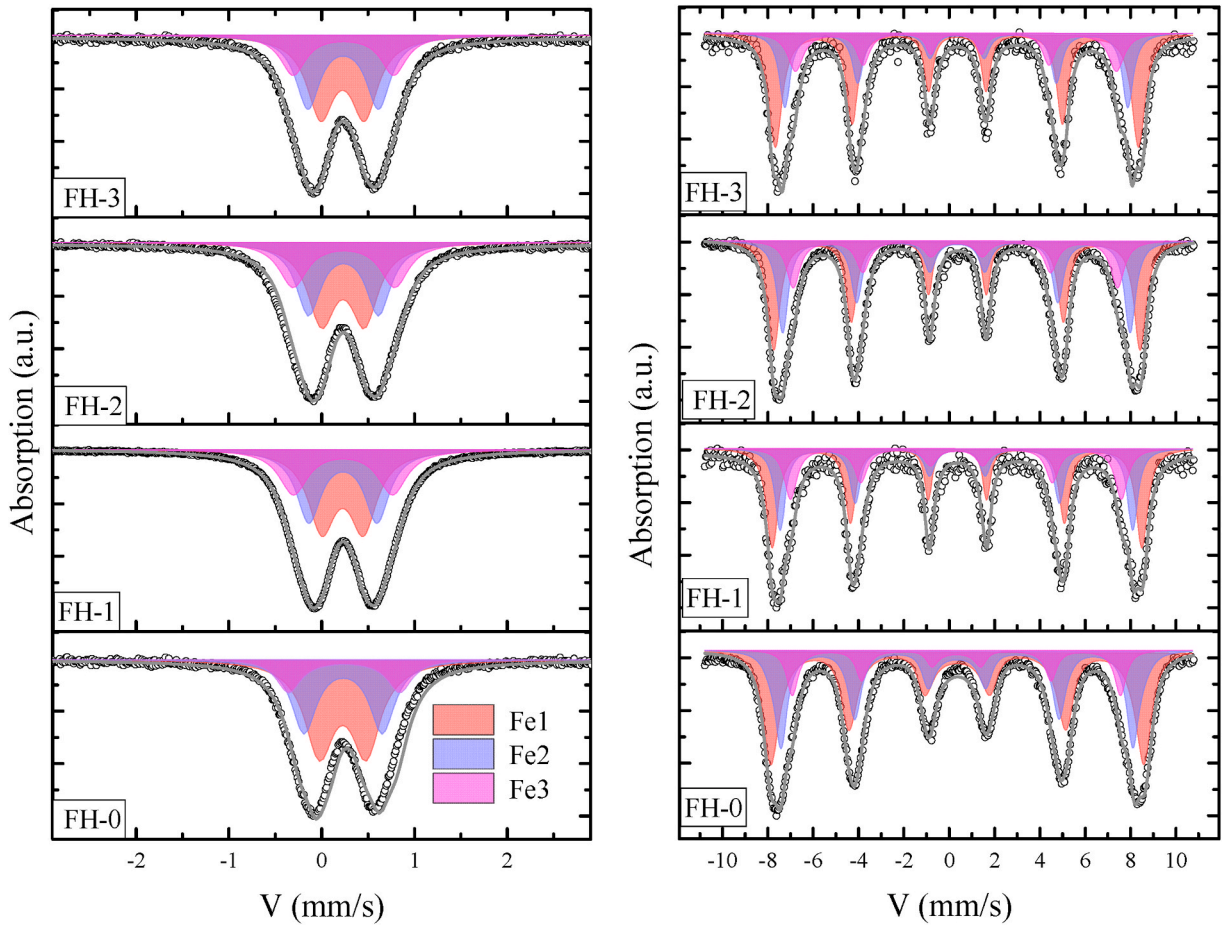

Fig. 3. Mössbauer spectra of the ferrihydrite samples obtained at 300 K (on the left) and at 4.2 K (on the right). Colored areas show partial spectra of three nonequivalent iron states.

5. Results and discussion

5.1. SPM blocking in the temperature dependences of the magnetization

Fig. 4–7 show the M(T) dependences obtained in fields H from 100 Oe to 30 kOe in the ZFC and FC modes. According to the general view of the data in Fig. 4–7, specifically, the relative positioning of the $M(T)_{ZFC}$ and $M(T)_{FC}$ dependences ($M_{FC} \geq M_{ZFC}$) and their irreversible behavior at temperatures below the characteristic temperature T_{irr}, it can be concluded that ferrihydrite nanoparticles in the samples undergo a transition from the SPM to blocked state. The $M(T)_{ZFC}$ dependences contain a pronounced maximum (we denote it as T_{max}), which generally shifts toward lower temperatures as the external field increases.

The $M(T)_{FC}$ dependence of sample FH-0 is nonmonotonic in fields of H = 100 and 1000 Oe (Fig. 4a and 5a) and the $M(T = 4.2\ K)_{FC}$ value is no higher than $M(T = T_{max})_{FC}$. The presence of the IPIs in this sample was confirmed in Ref. [44]. The described nonmonotonic nature of the $M(T)_{FC}$ dependences has been observed quite often in systems of interacting magnetic particles [9,10,15,16,19,28,44,45,60], so we can assume that the presence of a local $M(T)_{FC}$ minimum at temperatures below the transition to the blocked state (maxima in the $M(T)_{ZFC}$ dependence) is a manifestation of the IPIs. This may be due to the influence of fields induced by the magnetic moments of particles; then, the resulting effective field acting on the magnetic moment of a particle (or surface spins) will differ from the external field. As the latter increases, the contribution of the induced field becomes small and, as the temperature decreases, the $M(T)_{FC}$ dependences increase (see Fig. 6a and 7a). Another interesting fact is that, for sample FH-0, the characteristic temperature T_{irr} in a field of H = 1000 Oe is lower than T_{max} (see Fig. 5a). Meanwhile, the rest parameters in Fig. 4–7 behave conventionally: $T_{irr} > T_{max}$.

The $M(T)_{FC}$ dependences for coated ferrihydrite particles are no longer nonmonotonic. In the analysis of the ratio between the M_{FC} values at $T = T_{max}$ and low temperature (T = 4.2 K), we can state that, with an increase in the degree of coverage of ferrihydrite nanoparticles, the $M(T)_{FC}$ dependence increases faster with decreasing temperature (Fig. 4b and 5b). The $M(T)_{FC}$ evolution observed in the investigated sample series indirectly indicates the reducing effect of the IPIs in the SPM blocking processes.

There is also a distinctive feature of the shape of $M(T)_{ZFC}$ dependences in a moderate (0.1–1 kOe) fields, Fig. 4b and 5b. If one consider $M(T)_{ZFC}$ dependences as bell curves, the left (low-temperature) parts of them are almost identical for samples FH-1, FH-2, FH-3, meanwhile the peak width of these functions decreases with increase of amount of added AG. This can be related to diminishing influence of IPIs with increase of AG addition.

Eventually, according to the data from Fig. 4–7, the main trend for coated ferrihydrite nanoparticles is a decrease in characteristic temperatures T_{irr} and T_{max} (at H = const). This T_{irr} and T_{max} decrease is enhanced with an increase in the degree of coverage of particles (adding AG, see Sec.2): $T_{maxFH\text{-}0} > T_{maxFH\text{-}1}$, $T_{maxFH\text{-}1} > T_{maxFH\text{-}2}$, and $T_{maxFH\text{-}2} > T_{maxFH\text{-}3}$. It is reasonable to interpret this behavior as a consequence of weakening of the IPIs in the samples with the increasing amount of AG, through which the coating and spatial separation of ferrihydrite nanoparticles are implemented. Indeed, since particles in samples FH-1, FH-2, and FH-3 remain the same as in initial sample FH-0, then, in Eq. (3), the T_0 value changes (decreases with the increasing degree of coverage), while the right-hand side of Eq. (3) remains constant.

Table 1
Parameters obtained by processing of the Mössbauer spectra (Fig. 3). IS is the chemical shift relative to α-Fe, H_{hf} is the hyperfine field on iron nuclei, QS is the quadrupole splitting, W is the width of the Mössbauer line at the half height, and A is the relative occupancy of a position.

	IS, ±0.005 mm/s	H_{hf}, ±3 kOe	QS, mm/s ±0.01	W, ±0.01 mm/s	A, % ±0.03	position
FH-0	300 K					
	0.356	–	0.48	0.36	0.45	Fe1
	0.362	–	0.82	0.32	0.38	Fe2
	0.371	–	1.19	0.31	0.17	Fe3
	4.2 K					
	0.509	510	−0.01	0.73	0.48	Fe1
	0.496	481	−0.07	0.77	0.35	Fe2
	0.442	447	0.00	0.72	0.17	Fe3
FH-1	300 K					
	0.342	–	0.44	0.35	0.41	Fe1
	0.345	–	0.73	0.32	0.34	Fe2
	0.346	–	1.06	0.37	0.25	Fe3
	4.2 K					
	0.49	507	−0.02	0.38	0.44	Fe1
	0.475	484	−0.08	0.55	0.32	Fe2
	0.447	454	−0.05	0.68	0.24	Fe3
FH-2	300 K					
	0.345	–	0.46	0.35	0.41	Fe1
	0.351	–	0.75	0.32	0.34	Fe2
	0.354	–	1.09	0.36	0.24	Fe3
	4.2 K					
	0.486	503.2	−0.037	0.419	0.44	Fe1
	0.472	477.4	−0.081	0.6	0.35	Fe2
	0.437	445.6	−0.117	0.716	0.21	Fe3
FH-3	300 K					
	0.341	–	0.47	0.36	0.43	Fe1
	0.348	–	0.76	0.32	0.36	Fe2
	0.351	–	1.09	0.33	0.21	Fe3
	4.2 K					
	0.485	499	−0.04	0.43	0.51	Fe1
	0.466	471	−0.07	0.58	0.28	Fe2
	0.437	441	−0.02	0.44	0.21	Fe3

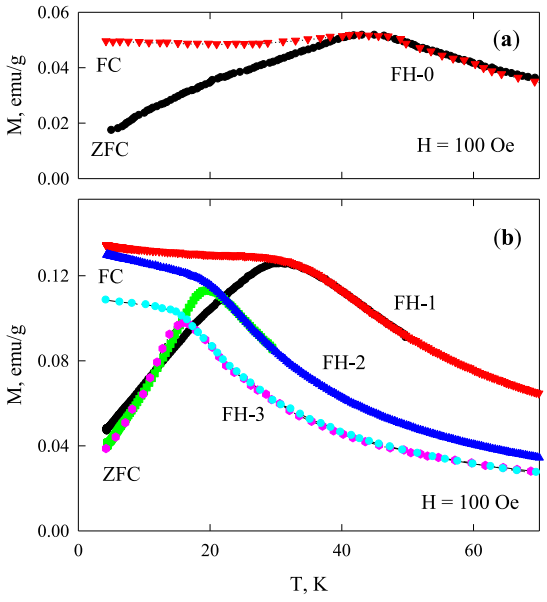

Fig. 4. $M(T)_{ZFC}$ and $M(T)_{FC}$ dependences of the magnetization in a field of H = 100 Oe for (a) sample FH-0 and (b) samples FH-1, FH-2, and FH-3.

Certainly, the sample preparation procedure does not guarantee that each particle is coated and spatially separated from other particles. It addition, it is not excluded that, with small AG additions, not particles but clusters of several particles are coated, but, with the increasing addition, the cluster size should decrease. Nevertheless, the above-described modification of the $(MT)_{FC}$ dependences and a monotonic decrease in the characteristic temperatures T_{max} and T_{irr} evidence for the weakening of the IPI effect with the increasing amount of added AG.

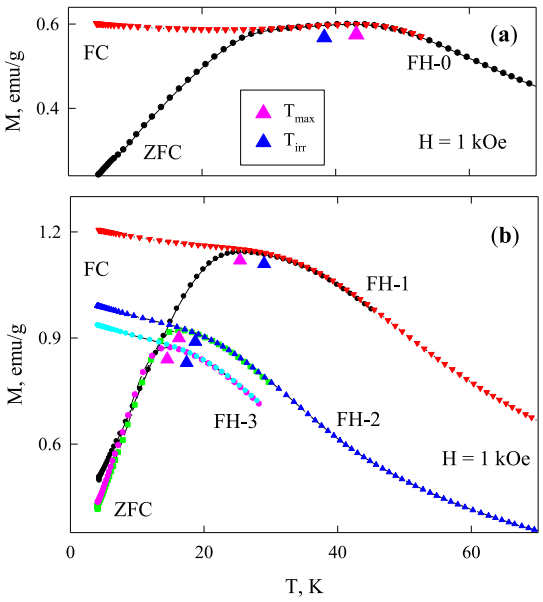

Fig. 5. $M(T)_{ZFC}$ and $M(T)_{FC}$ dependences of the magnetization in a field of H = 1 kOe for (a) sample FH-0 and (b) samples FH-1, FH-2, and FH-3. Characteristic temperatures T_{irr} of the irreversible behavior of the magnetization and $M(T)_{ZFC}$ maximum T_{max} are shown (see legend in (a)).

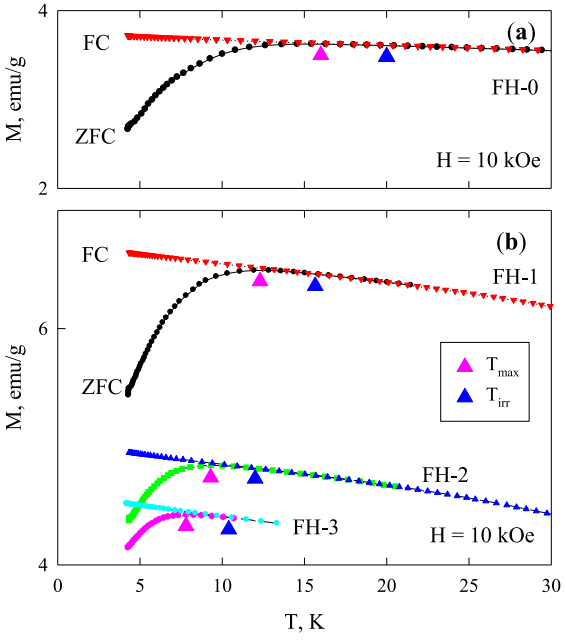

Fig. 6. $M(T)_{ZFC}$ and $M(T)_{FC}$ dependences of the magnetization in a field of H = 10 kOe for (a) sample FH-0 and (b) samples FH-1, FH-2, and FH-3. Characteristic temperatures T_{irr} and T_{max} are shown (see legend in (b)).

5.2. Analysis of the field dependences of the blocking temperature within RAM

Using the established behavior of the $M(T)_{ZFC}$ and $M(T)_{FC}$ dependences, at least three characteristic temperatures can be determined. These are the above-introduced temperatures T_{irr} and T_{max} and

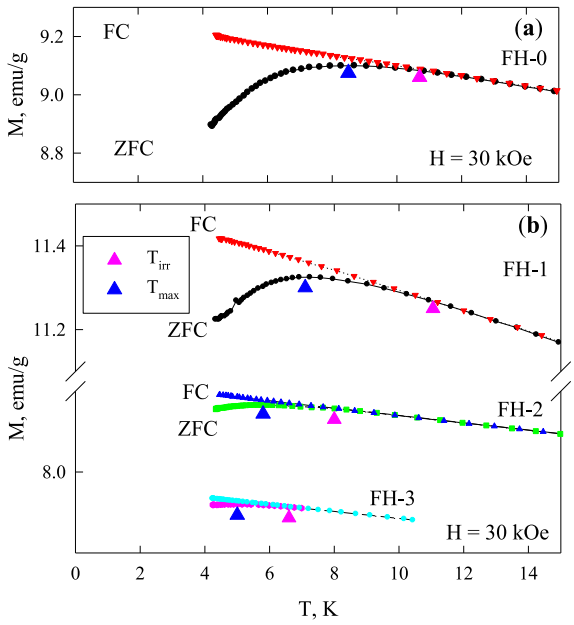

Fig. 7. $M(T)_{ZFC}$ and $M(T)_{FC}$ dependences of the magnetization in a field of H = 30 kOe for (a) sample FH-0 and (b) samples FH-1, FH-2, and FH-3 (b). Characteristic temperatures T_{irr} and T_{max} are shown (see legend in (b)).

temperature $<T_B>$ at which the dependence $f_D(T) = -d(M(T)_{FC} - M(T)_{ZFC})/dT$ has a maximum [27,43,57–61]. It is assumed that the temperature $<T_B>$ corresponds to the average particle size <D>. However, this approach not always yields the exact $<T_B>$ value. For example, the $f_D(T)$ dependence for samples FH-0 and FH-1 in fields of 100 and 1000 Oe is a complex nonmonotonic functions. According to our observations, there are the pronounced $f_D(T)$ maxima for samples FH-2 and FH-3 in fields of 100 and 1000 Oe. However, in fields of 10 kOe and stronger, the temperature $<T_B>$ is already below 4.2 K. On the other hand, it can be seen from the linear dependence of the SPM blocking temperature on the particle volume (Eq. (2) and (3)) that the temperature T_{irr} should correspond to the blocking of particles of the largest size. In our case, this is the size $D_{max} \approx 3.3$ nm. Then, the temperature T_{max} in the $M(T)_{ZFC}$ dependences should correspond to certain particle size D_m lying within $<D> \div D_{max}$, but, in this case, the choice of D_m is uncertain. Based on these considerations, in the further analysis of the effect of the external field on the SPM blocking temperature, we use the characteristic temperature T_{irr}, assuming it to correspond to the maximum particle size D_{max}.

Fig. 8a shows the $T_{irr}(H)$ dependences (symbols). The presented data cannot be described by Eq. (4), since it predicts a weaker decrease in the blocking temperature upon the field variation. To carry out a consistent analysis using Eq. (6), it is necessary to determine the minimum number of fitting parameters. The characteristic times τ_m and τ_0 were taken to be 10^2 and 10^{-12} s, respectively. The size D_{max} used is logical to be the same (3.3 nm) for all the samples. The M_S value for sample FH-0 was determined in Ref. [44] and amounts to 6 emu/g ($\mu_P \approx 170\ \mu_B$); we believe that the M_S values are identical for all the samples. The magnetic anisotropy constant K should also remain approximately the same for all the samples. The concentration x for sample FH-0 is obviously maximum: $x = 1$. It should decrease in the series FH-1, FH-2, FH-3. At the perfect coverage of each particle 3.3 nm in size on average with a 0.3-nm-thick AG layer, the calculated concentration is $x \approx 0.55$. However, for sample FH-3 with the maximum amount of added AG, at $x = 0.55$, the fitting requires a noticeably smaller K value for the stronger field (30 kOe) as compared with sample FH-0. Good agreement between two "reference" samples (FH-0 and FH-3) at the similar K values is obtained if we take $x \approx 1$ for FH-0 and $x \approx 0.65$ (± 0.05) for FH-3. This corresponds to a coating thickness of about 0.2 nm or, most likely,

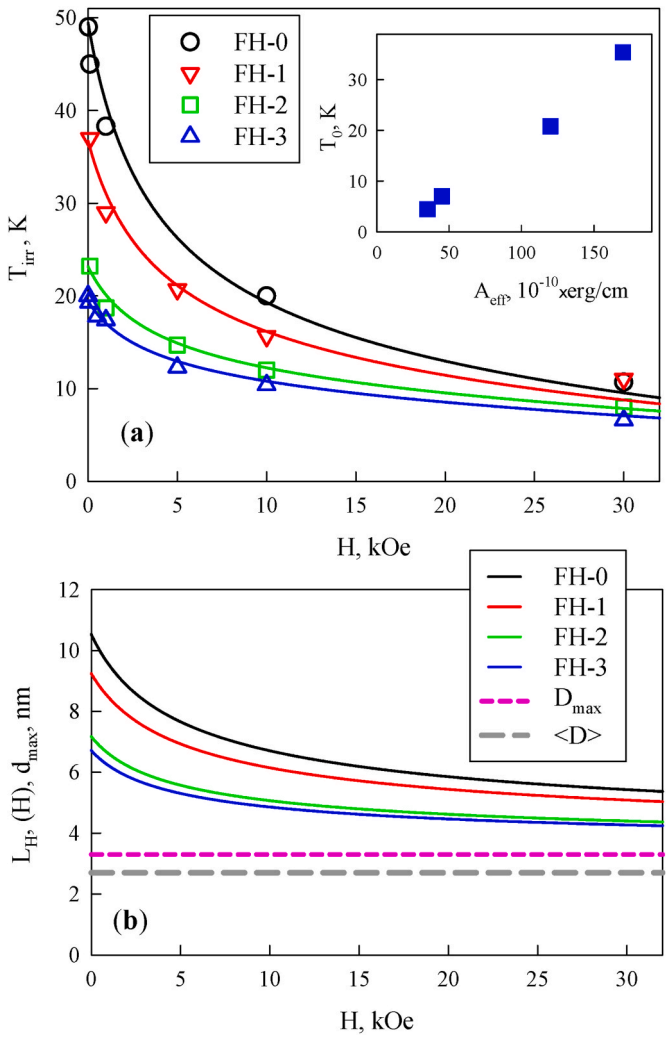

Fig. 8. (a) – Field dependences of the characteristic temperature T_{irr}. Dots show the experiment (according to the data from Fig. 4–7) and solid lines show the results of fitting by Eq. (6) with the fitting parameters given in Table 2. (b) – Field dependences of the parameter L_H (Eq. (5)); for comparison, the maximum particle size D_{max} and average particle size <D> are shown. Inset in (a): dependence of T_0 (in Eq. (3)) on A_{eff}.

indicates that not all particles are coated uniformly with AG. Based on these considerations, a value of $x = 0.65$ was used for sample FH-3 and the intermediate x values were used for the other two samples (see Table 2).

The K and x values determine basically the blocking temperature "level" in fairly strong fields, while, to describe the functional $T_B(H)$ dependence, it is necessary to "choose" the $L_H(H)$ function (Eq. (5)) determined by the parameters A_{eff} and C. The larger A_{eff} value and the smaller C value correspond to the stronger IPI effect. Thus, the main variable parameters are A_{eff} and C. Upon their variation, we obtain two possible sets of these parameters that describe satisfactorily the experimental data; in this case, the $L_H(H)$ dependences are identical and the $L_H(H = 0)$ values are similar. In the first variant, both parameters A_{eff} and C decrease as AG is added. A decrease in A_{eff} with the decreasing IPI contribution is logical, while a decrease in the parameter C is difficult to explain. In the other variant, satisfactory agreement with the experimental data is obtained if the C value remains approximately the same for all the samples and A_{eff} decreases monotonically as AG is added. The results of this fitting variant are illustrated in Fig. 8a (solid lines). The parameters A_{eff}, C, and K are given in Table 2. We note that the K variation was no more than 5%. Good agreement of the calculated

Table 2
Parameters of the investigated samples used in the simulation of the $T_{irr}(H)$ dependences in Fig. 6

Sample	x (±0.05)	K, erg/cm^3 (±2%)	C, erg/cm^3 (±5%)	A_{eff}, erg/cm (±5%)	L_0(H = 0), nm (±2%)	N_p in a cluster at H = 0	N_p in a cluster at H = 30 kOe
FH-0	1.0	$2.05{\cdot}10^6$	$6.5{\cdot}10^4$	$170{\cdot}10^{-10}$	10.5	59	8
FH-1	0.85	$2.0{\cdot}10^6$	$6.8{\cdot}10^4$	$120{\cdot}10^{-10}$	9.2	40	7
FH-2	0.7	$2.0{\cdot}10^6$	$6.0{\cdot}10^4$	$45{\cdot}10^{-10}$	7.2	19	4
FH-3	0.65	$1.9{\cdot}10^6$	$6.0{\cdot}10^4$	$35{\cdot}10^{-10}$	6.7	15	4

dependences with a decrease in the characteristic temperature T_{irr} observed experimentally in the growing external field, as well as the reasonable A_{eff} and C values [21,27,28], testify to the adequacy of the fitting. The $L_H(H)$ functions obtained during fitting of the $T_{irr}(H)$ data are presented in Fig. 8b (solid lines). For comparison, the maximum D_{max} and average <D> particle sizes are shown (horizontal dashed lines).

The analysis of the behavior of the fitting parameters allows us to draw the following conclusions. The size $L_H(H = 0)$ (see Fig. 8b and Table 2) of the cluster in which the behaviors of the magnetic moments of particles are correlated exceeds both the average and the maximum particle size. In fairly strong external fields, $L_H(H)$ approaches the D_{max} value (see Fig. 8b), according to (5). In zero external field, the $L_H(H = 0)$ value is four times as much as <D> in sample FH-0 and the ratio $L_H(H = 0)/<D>$ decreases monotonically in the series FH-1, FH-2, FH-3. In this case, the parameter A_{eff} decreases monotonically as well. Table 2 also lists the numbers of medium-sized particles in a cluster in zero field and a field of H = 30 kOe. As the amount of added AG increases, the number of particles in the cluster decreases. This indirectly indicates that, when ferrihydrite particles are coated with AG, the IPI intensity decreases; however, the IPI effect still remains, even in sample FH-3.

Let us pay attention to the obtained effective magnetic anisotropy constant K (Table 2). Within the RAM, K is the anisotropy constant of an individual particle, with the already subtracted IPI effect. A value of $K \approx 2.0{\cdot}10^6$ erg/cm^3 exceeds significantly the typical bulk magnetic anisotropy constants of magnetically ordered oxides. In the absence of noticeable shape anisotropy of ferrihydrite particles (Fig. 1), this is indicative of a significant contribution of the surface magnetic anisotropy [21,22,38,41,45,58,59,62–66].

On the other hand, knowing the magnetic anisotropy constant of an individual particle, one can determine the parameter T_0 in Eq. (3). Since the T_0 value characterizes the IPI intensity, there should be a linear correlation between this value and the parameter A_{eff} in the RAM. Indeed, the linear correlation exists: see the inset in Fig. 8a, where dots obey well the linear dependence. This additionally confirms the validity of the RAM in the above quantitative description of the field dependences of the SPM blocking temperature.

Speaking about the nature of the magnetic IPIs in the investigated ferrihydrite systems, the estimation of the energy of the dipole–dipole interaction between two ferrihydrite particles (with a size of ~3 nm and a magnetic moment of about 150–200 Bohr magnetons [13,44,45,55]) that are in contact with each other yields a value much less than 1 K [13]. Even if 10–12 nearest neighbors are taken into account, then the energy of the dipole–dipole interactions is no higher than 10 K. Although this value is qualitatively consistent with the temperature T_0 (inset in Fig. 6a) for samples FH-2 and FH-3, it cannot explain the SPM blocking processes in the other two samples (FH-0 and FH-1). Therefore, it is necessary to seek other magnetic IPI mechanisms responsible for the growth of the SPM blocking temperatures, especially for initial FH-0 sample, for example, exchange (superexchange) or indirect interactions between iron atoms of neighboring particles. This topic will be the object of further studies.

6. Conclusions

Thus, the ferrihydrite powder systems with different degrees of coverage of ferrihydrite nanoparticles (the average size is ~2.6 nm and the maximum size is 3.3 nm) with the arabinogalactan molecular layer were synthesized. According to the XPS data, an increase in the effective coating thickness with the degree of addition of AG was stated. The Mössbauer spectroscopy study showed no significant changes in the local environment of iron (III) atoms and the properties of individual ferrihydrite particles remained identical. It was shown that the coating of ferrihydrite nanoparticles reduces the SPM blocking temperature from ~49 K for uncoated particles (pure synthetic ferrihydrite) to ~16 K in a low field (100 Oe), which occurs monotonically as the degree of coverage growth, obviously, due to the weakening effect of the interparticle magnetic interactions on the SPM blocking processes. The field dependence of the SPM blocking temperature for the synthesized sample series was analyzed within the RAM [27,28], which considers a cluster of particles the magnetic moments of which behave in a correlated manner; the cluster size L_H depends on the external field. Good agreement between the experimental data and RAM calculation and the results of the analysis convincingly proved that the role of the interparticle magnetic interactions weakens with the increasing degree of particle coverage. The cluster size L_H (for "pure" ferrihydrite L_H in a weak field, it exceeds the average particle size by a factor of four) decreases by several times for coated particles. Thus, it was experimentally shown that the interparticle magnetic interactions affect significantly the SPM blocking of the magnetic moments of synthetic ferrihydrite nanoparticles and the coating of particles with arabinogalactan is an efficient method for tuning (downward) the effect of the interparticle magnetic interactions.

Funding

This study was supported by his work was supported by the Russian Science Foundation, project no. 22-72-00134.

Credit author statement

A.A. Krasikov: Project administration, Funding acquisition, Conceptualization, Writing – original draft, Writing – review and editing, Yu.V. Knyazev: Writing – original draft, Visualization, Investigation, D.A. Balaev: Conceptualization, Writing – original draft, Writing – review and editing, D.A. Velikanov: Investigation, S.V. Stolyar: Methodology/Study design, Investigation, Formal analysis, Yu.L. Mikhlin: Investigation, R.N.Yaroslavtsev: Investigation, Resources, R.S. Iskhakov: Supervision, Data curation.

Declaration of competing interest

The authors declare the following financial interests/personal relationships which may be considered as potential competing interests: Alexandr Krasikov reports financial support was provided by Russian Science Foundation, project no. 22-72-00134.

Data availability

No data was used for the research described in the article.

Acknowledgments

Authors thank to A.D. Balaev, S.V. Komogortsev for fruitful

discussions and M.N. Volochaev for TEM studies. The TEM study and XPS measurements were carried out on the equipment of the Krasnoyarsk Territorial Center for Collective Use, Krasnoyarsk Scientific Center, Siberian Branch, Russian Academy of Sciences.

References

[1] J. Mohapatra, M. Xing, J.P. Liu, Inductive thermal effect of ferrite magnetic nanoparticles, Materials 19 (2019) 3208, https://doi.org/10.3390/ma12193208.

[2] X. Batlle, C. Moya, M. Escoda-Torroella, Ò. Iglesias, A.F. Rodríguez, A. Labarta, J. Magn. Magn Mater. 543 (2022), 168594, https://doi.org/10.1016/j.jmmm.2021.168594.

[3] S.I. Ahmad, J. Magn. Magn Mater. 562 (2022), 169840, https://doi.org/10.1016/j.jmmm.2022.169840.

[4] S. Mørup, M.B. Madsen, J. Franck, J. Villadsen, C.J.W. Koch, J. Magn. Magn Mater. 40 (1983) 163–174, https://doi.org/10.1016/0304-8853(83)90024-0.

[5] S. Morup, E. Tronc, Phys. Rev. Lett. 72 (1994) 3278.

[6] C. Djurberg, P. Svedlindh, P. Nordblad, M.F. Hansen, F. Bødker, S. Mørup, Dynamics of an interacting particle system: evidence of critical slowing down, Phys. Rev. Lett. 79 (N25) (1997) 5154–5167.

[7] F. Bødker, M.F. Hansen, C. Bender Koch, S. Mørup, Particle interaction effects in antiferromagnetic NiO nanoparticles, J. Magn. Magn Mater. 221 (2000) 32–36, https://doi.org/10.1016/S0304-8853(00)00392-9.

[8] G.F. Goya, T.S. Berquó, F.C. Fonseca, M.P. Morales, Static and dynamic magnetic properties of spherical magnetite nanoparticles, J. Appl. Phys. 94 (2003) 3520–3528, https://doi.org/10.1063/1.1599959.

[9] J.M. Vargas, W.C. Nunes, L.M. Socolovsky, M. Knobel, D. Zanchet, Effect of dipolar interaction observed in iron-based nanoparticles, Phys. Rev. B 72 (2005), 184428, https://doi.org/10.1103/PhysRevB.72.184428.

[10] C.A.M. Vieira, R. Cabreira Gomes, F.G. Silva, A.L. Dias, R. Aquino, A.F.C. Campos, J. Depeyrot, Blocking and remanence properties of weakly and highly interactive cobalt ferrite based nanoparticles, J. Phys. Condens. Matter 31 (2019) 17580 1, https://doi.org/10.1088/1361-648X/ab0353.

[11] E.L. Duarte, R. Itri, E. Lima Jr., M.S. Baptista, T.S. Berquó, G.F. Goya, Large magnetic anisotropy in ferrihydrite nanoparticles synthesized from reverse micelles, Nanotechnology 17 (2006) 5549–5555, https://doi.org/10.1088/0957-4484/17/22/004.

[12] T.S. Berquó, J.J. Erbs, A. Lindquist, R.L. Penn, S.K. Banerjee, Effects of magnetic interactions in antiferromagnetic ferrihydrite particles, J. Phys. Condens. Matter 21 (2009), 176005, https://doi.org/10.1088/0953-8984/21/17/176005.

[13] S. Mørup, D.E. Madsen, C. Fradsen, C.R.H. Bahl, M.F. Hansen, Experimental and theoretical studies of nanoparticles of antiferromagnetic materials, J. Phys. Condens. Matter 19 (2007), 213202, https://doi.org/10.1088/0953-8984/19/21/213202.

[14] A.M. Pereira, C. Pereira, A.S. Silva, D.S. Schmool, C. Freire, J.-M. Grenèche, J. P. Araújo, Unravelling the effect of interparticle interactions and surface spin canting in γ-Fe2O3@SiO2 superparamagnetic nanoparticles, J. Appl. Phys. 109 (2011), 114319, https://doi.org/10.1063/1.3583652.

[15] M. Suzuki, S.I. Fullem, I.S. Suzuki, L. Wang, Ch-J. Zhong, Observation of superspin-glass behavior in Fe_3O_4 nanoparticles, Phys. Rev. B 79 (2009), 024418, https://doi.org/10.1103/PhysRevB.79.024418.

[16] D. Caruntu, G. Caruntu, ChJ. O'Connor, Magnetic properties of variable-sized Fe_3O_4 nanoparticles synthesized from non-aqueous homogeneous solutions of polyols, J. Phys. D Appl. Phys. 40 (2007) 5801–5809, https://doi.org/10.1088/0022-3727/40/19/001.

[17] H. Shim, P. Dutta, M.S. Seehra, J. Bonevich, Size dependence of the blocking temperatures and electron magnetic resonance spectra in NiO nanoparticles, Solid State Commun. 145 (2008) 192–196, https://doi.org/10.1016/j.ssc.2007.10.026.

[18] S. Mørup, M.F. Hansen, C. Frandsen, Magnetic interactions between nanoparticles, Beilstein J. Nanotechnol. 1 (2010) 182–190, https://doi.org/10.3762/bjnano.1.22.

[19] K. Nadeem, H. Krenn, T. Traussnig, R. Würschum, D.V. Szabó, I. Letofsky-Papst, Effect of dipolar and exchange interactions on magnetic blocking of maghemite nanoparticles, J. Magn. Magn Mater. 323 (2011) 1998–2004, https://doi.org/10.1016/j.jmmm.2011.02.041.

[20] V. Russier, Blocking temperature of interacting magnetic nanoparticles with uniaxial and cubic anisotropies from Monte Carlo simulations, J. Magn. Magn Mater. 409 (2016) 50–55, https://doi.org/10.1016/j.jmmm.2016.02.070.

[21] D.A. Balaev, S.V. Semenov, A.A. Dubrovskiy, S.S. Yakushkin, V.L. Kirillov, O. N. Martyanov, Superparamagnetic blocking of an ensemble of magnetite nanoparticles upon interparticle interactions, J. Magn. Magn Mater. 440 (2017) 199–202, https://doi.org/10.1016/j.jmmm.2016.12.046.

[22] M. Vasilakaki, F. Gemenetzi, E. Devlin, D.K. Yi, S.N. Riduan, S.S. Lee, J.Y. Ying, G. C. Papaefthymiou, K.N. Trohidou, Size effects on the magnetic behavior of γ-Fe2O3 core/SiO2 shell nanoparticle, assemblies, J. Magn. Magn Mater. 522 (2021), 167570, https://doi.org/10.1016/j.jmmm.2020.167570.

[23] K. Nadeem, M. Kamran, A. Javed, F. Zeb, S.S. Hussain, M. Mumtaz, H. Krenn, D. V. Szabo, U. Brossmann, X. Mu, Role of surface spins on magnetization of Cr_2O_3 coated γ-Fe_2O_3 nanoparticles, Solid State Sci. 83 (2018) 43–48, https://doi.org/10.1016/j.solidstatesciences.2018.07.006.

[24] S.V. Komogortsev, R.S. Iskhakov, V.A. Fel'k, Fractal dimension effect on the magnetization curves of exchange-coupled clusters of magnetic nanoparticles, J. Exp. Theor. Phys. 128 (2019) 754–760, https://doi.org/10.1134/S1063776119040095.

[25] S.V. Komogortsev, V.A. Fel'k, O.A. Li, The magnetic dipole-dipole interaction effect on the magnetic hysteresis at zero temperature in nanoparticles randomly dispersed within a plane, J. Magn. Magn Mater. 473 (2019) 410–415, https://doi.org/10.1016/j.jmmm.2018.10.091.

[26] L.L. Afremov, S.V. Anisimov, I.G. Iliushin, Modeling of the blocking temperature of a system of core/shell nanoparticles, Chin. J. Phys. 70 (2021) 324–335, https://doi.org/10.1016/j.cjph.2020.06.022.

[27] W.C. Nunes, L.M. Socolovsky, J.C. Denardin, F. Cebollada, A.L. Brandl, M. Knobel, Role of magnetic interparticle coupling on the field dependence of the superparamagnetic relaxation time, Phys. Rev. B 72 (2005), 212413, https://doi.org/10.1103/PhysRevB.72.212413.

[28] M. Knobel, W.C. Nunes, H. Winnischofer, T.C.R. Rocha, L.M. Socolovsky, C. L. Mayorga, D. Zanchet, Effects of magnetic interparticle coupling on the blocking temperature of ferromagnetic nanoparticle arrays, J. Non-Cryst. Solids 353 (2007) 743–747, https://doi.org/10.1016/j.jnoncrysol.2006.12.037.

[29] F. Fabris, Kun-Hua Tu, C.A. Ross, W.C. Nunes, Influence of dipolar interactions on the magnetic properties of superparamagnetic particle systems, J. Appl. Phys. 126 (2019), 173905, https://doi.org/10.1063/1.512559.

[30] L. Néel, Superantiferromagnetism in small particles, C.R. Acad. Sci. Paris 253 (1961) 203.

[31] C. Gilles, P. Bonville, K.K.W. Wong, S. Mann, Non-Langevin behaviour of the uncompensated magnetization in nanoparticles of artificial ferritin, Eur. Phys. J. B 17 (2000) 417, https://doi.org/10.1007/s100510070121.

[32] C. Gilles, P. Bonville, H. Rakoto, J.M. Broto, K.K.W. Wong, S. Mann, Magnetic hysteresis and superantiferromagnetism in ferritin nanoparticles, J. Magn. Magn Mater. 241 (2002) 430, https://doi.org/10.1016/S0304-8853(01)00461-9.

[33] A. Punnoose, T. Phanthavady, M. Seehra, N. Shah, G. Huffman, Magnetic properties of ferrihydrite nanoparticles doped with Ni, Mo, and Ir, Phys. Rev. B 69 (5) (2004), 054425, https://doi.org/10.1103/PhysRevB.69.054425.

[34] N.J.O. Silva, V.S. Amaral, L.D. Carlos, Relevance of magnetic moment distribution and scaling law methods to study the magnetic behavior of antiferromagnetic nanoparticles: application to ferritin, Phys. Rev. B 71 (2005), 184408, https://doi.org/10.1103/PhysRevB.71.184408.

[35] S.D. Tiwari, K.P. Rajeev, Effect of distributed particle magnetic moments on the magnetization of NiO nanoparticles, Solid State Commun. 152 (2012) 1080, https://doi.org/10.1016/j.ssc.2012.03.003.

[36] Ch Rani, S.D. Tiwari, Superparamagnetic behavior of antiferromagnetic six lines ferrihydrite nanoparticles, Physica B 513 (2017) 58, https://doi.org/10.1016/j.physb.2017.02.036.

[37] S.I. Popkov, A.A. Krasikov, A.A. Dubrovskiy, M.N. Volochaev, V.L. Kirillov, O. N. Martyanov, D.A. Balaev, Size effects in the formation of an uncompensated ferromagnetic moment in NiO nanoparticles, J. Appl. Phys. 126 (2019), 103904, https://doi.org/10.1063/1.5109054.

[38] S.I. Popkov, A.A. Krasikov, D.A. Velikanov, V.L. Kirillov, O.N. Martyanov, D. A. Balaev, Formation of the magnetic subsystems in antiferromagnetic NiO nanoparticles using the data of magnetic measurements in fields up to 250 kOe, J. Magn. Magn Mater. 483 (2019) 21, https://doi.org/10.1016/j.jmmm.2019.03.004.

[39] C. Parmar, G.S. Parmar, Structural and magnetic properties of six-line ferrihydrite nanoparticles, J. Supercond. Nov. Magnetism 33 (2020) 441–444, https://doi.org/10.1007/s10948-019-05200-x.

[40] T. Iimor, Y. Imamoto, N. Uchida, Y. Kikuchi, K. Honda, T. Iwahashi, Y. Ouch, Magnetic moment distribution in nanosized antiferromagnetic NiO, J. Appl. Phys. 127 (2020), 023902, https://doi.org/10.1063/1.5135335.

[41] D.A. Balaev, A.A. Krasikov, S.I. Popkov, S.V. Semenov, M.N. Volochaev, D. A. Velikanov, V.L. Kirillov, O.N. Martyanov, Uncompensated magnetic moment and surface and size effects in few-nanometer antiferromagnetic NiO particles, J. Magn. Magn Mater. 539 (2021), 168343, https://doi.org/10.1016/j.jmmm.2021.168343.

[42] M. Tadić, M. Panjan, D. Marković, NiO/SiO_2 nanostructure and the magnetic moment of NiO nanoparticles, Mater. Lett. 64 (2010) 2129–2131, https://doi.org/10.1016/j.matlet.2010.07.006.

[43] D.A. Balaev, A.A. Krasikov, S.V. Stolyar, R.S. Iskhakov, V.P. Ladygina, R. N. Yaroslavtsev, O.A. Bayukov, A.M. Vorotynov, M.N. Volochaev, A.A. Dubrovskii, Change in the magnetic properties of nanoferrihydrite with an increase in the volume of nanoparticles during low-temperature annealing, Phys. Solid State 58 (2016) 1782, https://doi.org/10.1134/S1063783416090092.

[44] YuV. Knyazev, D.A. Balaev, S.V. Stolyar, A.A. Krasikov, O.A. Bayukov, M. N. Volochaev, R.N. Yaroslavtsev, V.P. Ladygina, D.A. Velikanov, R.S. Iskhakov, Interparticle magnetic interactions in synthetic ferrihydrite: Mössbauer spectroscopy and magnetometry study of the dynamic and static manifestations, J. Alloys Compd. 889 (2021), 161623, https://doi.org/10.1016/j.jallcom.2021.161623.

[45] D.A. Balaev, S.V. Stolyar, YuV. Knyazev, R.N. Yaroslavtsev, A.I. Pankrats, A. M. Vorotynov, A.A. Krasikov, D.A. Velikanov, O.A. Bayukov, V.P. Ladygina, R. S. Iskhakov, Results Phys. 35 (2022), 105340, https://doi.org/10.1016/j.rinp.2022.105340.

[46] M.S. Seehra, V.S. Babu, A. Manivannan, J.W. Lynn, Neutron scattering and magnetic studies of ferrihydrite nanoparticles, Phys. Rev. B 61 (2000) 3513–3518, https://doi.org/10.1103/PhysRevB.61.3513.

[47] YuV. Knyazev, D.A. Balaev, R.N. Yaroslavtsev, A.A. Krasikov, D.A. Velikanov, YuL. Mikhlin, M.N. Volochaev, O.A. Bayukov, S.V. Stolyar, R.S. Iskhakov, Tuning the interparticle interactions in ultrafine ferrihydrite nanoparticles, Advances in Nano Research 12 (2022) 605, https://doi.org/10.12989/anr.2022.12.6.605.

[48] S.V. Stolyar, R.N. Yaroslavtsev, A.V. Tyumentseva, S.V. Komogortsev, E. S. Tyutrina, A.T. Saitova, YuV. Gerasimova, D.A. Velikanov, M.V. Rautskii, R.

S. Iskhakov, Manifestation of stoichiometry deviation in silica-coated magnetite nanoparticles, J. Phys. Chem. C 126 (2022) 7510–7516.
[49] M.C. Biesinger, B.P. Payne, A.P. Grosvenor, L.W.M. Lau, A.R. Gerson, R. St, C. Smart, Resolving surface chemical states in XPS analysis of first row transition metals, oxides and hydroxides: Cr, Mn, Fe, Co and Ni, Appl. Surf. Sci. 257 (2011) 2717–2730, https://doi.org/10.1016/j.apsusc.2010.10.051.
[50] E.M. Chudnovsky, W.M. Saslow, R.A. Scrota, Ordering in ferromagnets with random anisotropy, Phys. Rev. B 33 (1986) 251.
[51] R.H. Victora, Predicted time dependence of the switching field for magnetic materials, Phys. Rev. Lett. 63 (1989) 457–460, 10.1103/PhysRevLett.63.457.
[52] M. Mallet, K. Barthélémy, C. Ruby, A. Renard, S. Naille, Investigation of phosphate adsorption onto ferrihydrite by X-ray Photoelectron Spectroscopy, J. Colloid Interface Sci. 407 (2013) 95–101, https://doi.org/10.1016/j.jcis.2013.06.049.
[53] A.P. Grosvenor, B.A. Kobe, N.S. McIntyre, S. Tougaard, W.N. Lennard, Use of QUASES^{TM}/XPS measurements to determine the oxide composition and thickness on an iron substrate, Surf. Interface Anal. 36 (2004) 632–639.
[54] J. Zhao, F.E. Huggins, Z. Feng, G.P. Huffman, Surface-induced superparamagnetic relaxation in nanoscale ferrihydrite particles, Phys. Rev. B 54 (1996) 3404–3407.
[55] S.V. Stolyar, D.A. Balaev, V.P. Ladygina, A.A. Dubrovskiy, A.A. Krasikov, S. I. Popkov, O.A. Bayukov, YuV. Knyazev, R.N. Yaroslavtsev, M.N. Volochaev, R. S. Iskhakov, K.G. Dobretsov, E.V. Morozov, O.V. Falaleev, E.V. Inzhevatkin, O. A. Kolenchukova, I.A. Chizhova, Bacterial ferrihydrite nanoparticles: preparation, magnetic properties, and application in medicine, J. Supercond. Nov. Magnetism 31 (2018) 2297, https://doi.org/10.1007/s10948-018-4700-1.
[56] S.V. Stolyar, R.N. Yaroslavtsev, R.S. Iskhakov, O.A. Bayukov, D.A. Balaev, A. A. Dubrovskii, A.A. Krasikov, V.P. Ladygina, A.M. Vorotynov, M.N. Volochaev, Magnetic and resonance properties of ferrihydrite nanoparticles doped with cobalt, Phys. Solid State 59 (3) (2017) 555–563, https://doi.org/10.1134/S1063783417030301.
[57] J. Fock, M.F. Hansen, C. Frandsen, S. Mørup, On the interpretation of Mössbauer spectra of magnetic nanoparticles, J. Magn. Magn Mater. 445 (2018) 11–21, https://doi.org/10.1016/j.jmmm.2017.08.070.
[58] YuV. Knyazev, D.A. Balaev, V.L. Kirillov, O.A. Bayukov, O.N. Mart'yanov, Mössbauer spectroscopy study of the superparamagnetism of ultrasmall ε-Fe_2O_3 nanoparticles, JETP Lett. 108 (2018) 527–531, https://doi.org/10.1134/S0021364018200092.
[59] YuV. Knyazev, D.A. Balaev, S.V. Stolyar, O.A. Bayukov, R.N. Yaroslavtsev, V. P. Ladygina, D.A. Velikanov, R.S. Iskhakov, Magnetic anisotropy and core-shell structure origin of the biogenic ferrihydrite nanoparticles, J. Alloys Compd. 851 (2021), 156753, https://doi.org/10.1016/j.jallcom.2020.156753.
[60] J.C. Denardin, A.L. Brandl, M. Knobel, P. Panissod, A.B. Pakhomov, H. Liu, X. X. Zhang, Thermoremanence and zero-field-cooled/field-cooled magnetization study of $Co_x(SiO_2)_{1-x}$ granular films, Phys. Rev. B 65 (2002), 064422, https://doi.org/10.1103/PhysRevB.65.064422.
[61] M. Knobel, W.C. Nunes, L.M. Socolovsky, E. De Biasi, J.M. Vargas, J.C. Denardin, Superparamagnetism and other magnetic features in granular materials: a review on ideal and real systems, J. Nanosci. Nanotechnol. 8 (2008) 2836–2857, https://doi.org/10.1166/jnn.2008.017.
[62] D.A. Balaev, A.A. Krasikov, S.I. Popkov, A.A. Dubrovskiy, S.V. Semenov, D. A. Velikanov, V.L. Kirillov, O.N. Martyanov, Features of the quasi-static and dynamic magnetization switching in NiO nanoparticles: manifestation of the interaction between magnetic subsystems in antiferromagnetic nanoparticles, J. Magn. Magn Mater. 515 (2020), 167307, https://doi.org/10.1016/j.jmmm.2020.167307.
[63] J. Mohapatra, M. Xing, J. Elkins, J. Beatty, J Ping Liu, Size-dependent magnetic hardening in $CoFe_2O_4$ nanoparticles: effects of surface spin canting, J. Phys. D Appl. Phys. 53 (2020), 504004, https://doi.org/10.1088/1361-6463/abb622.
[64] D.A. Balaev, I.S. Poperechny, A.A. Krasikov, S.V. Semenov, S.I. Popkov, Y. V. Knyazev, V.L. Kirillov, S.S. Yakushkin, O.N. Martyanov, YuL. Raikher, Dynamic remagnetisation of $CoFe_2O_4$ nanoparticles: thermal fluctuational thawing of anisotropy, J. Phys. D Appl. Phys. 54 (2021), 275003, https://doi.org/10.1088/1361-6463/abf371.
[65] A. Aharoni, Surface anisotropy in micromagnetics, J. Appl. Phys. 61 (1987) 3302, https://doi.org/10.1063/1.338890.
[66] F. Bødker, S. Mørup, S. Linderoth, Surface effects in metallic iron nanoparticles, Phys. Rev. Lett. 72 (1994) 282, https://doi.org/10.1103/PhysRevLett.72.282.